ADVANCED ENERGY MATERIALS

Supporting Information

for *Adv. Energy Mater.,* DOI: 10.1002/aenm.202203122

Impact of Reversible Proton Insertion on the Electrochemistry of Electrode Materials Operating in Mild Aqueous Electrolytes: A Case Study with TiO_2

Nikolina Makivić, Kenneth D. Harris, Jean-Marie Tarascon, Benoît Limoges, and Véronique Balland**

Supporting Information

Impact of reversible proton insertion on the electrochemistry of electrode materials operating in mild aqueous electrolytes: a case study with TiO_2

Nikolina Makivić, Kenneth D. Harris, Jean-Marie Tarascon, Benoît Limoges, Véronique Balland**

1. Glossary of symbols

Latin lower case d: distance from left edge of the analysed image area d_f : mesoporous film thickness d_a : compact equivalent film thickness g: Frumkin parameter i: current $i_{f,index}$: faradaic charge storage current of the electrochemical reaction specified by the index i_g : galvanostatic current applied in potentiometry i_c : capacitive current k_{index} : rate constant of the process specified by *index* k_{index}^0 : standard heterogeneous rate constant of electrochemical reaction specified by the index t: time t_{inv} : time when the applied galvanostatic current is inverted $t_{\max}$: the maximal time in potentiometry z: distance perpendicular to the underlying planar conductive electrode y: distance parallel to a fixed position on the underlying planar conductive electrode **Capital Latin** C_i : volume concentration of species i C_i^0 : initial bulk volume concentration of species i Γ_0^0 : maximal surface concentration of redox-active sites in the film Γ_i : surface concentration of redox-active species i in the film C_e^0 : maximal concentration of electrons that can be injected in the semiconductive film C_f : total capacitance of the film C_{dl} : differential double-layer capacitance C_{chem} : the chemical capacitance associated to the exponential filling/emptying of the conduction band D_i : diffusion coefficient of species i E : potential of the electrode E_i : initial potential	E_i^0 : standard potential of electrochemical reaction i E_{cb} : conduction band potential of the film F: Faraday constant K_a: acid dissociation constant R: gas constant S: geometrical electrode surface area S_a: specific electroactive surface area T: absolute temperature u: electrolyte convection velocity **Greek lower case** α: transfer coefficient β: parameter characterizing the transition from the insulating to conductive state of the film δ: thickness of the diffusion-convection layer θ: fraction of film protonation

2. Models

2.1. One- (1D) and two-dimensional (2D) one-compartment models

The 1D and 2D one-compartment models used for the numerical simulations both correspond to a simplified version of the two-compartment model we published previously.[S1,S2] The schematic representation of these models is illustrated in Scheme S1, which shows the transition from a basic side-view representation of the mesoporous GLAD-TiO_2 electrode to a two-compartment model, and then to a simpler one-compartment representation when the mass transport in the TiO_2 film can be considered non rate-limiting. Briefly, the two-compartment model assumes that the porous semiconductive TiO_2 film of geometric surface area S, thickness d_f, and accessible area S_a can be represented by a flat TiO_2 film of geometric surface S_a and thickness d_a, through which protons diffuse according to an isotropic finite diffusion mass transport (*vide infra*). Outside the film (*i.e.*, in the electrolyte compartment), the mass transport of soluble species occurs by semi-infinite diffusion-convection towards the geometric surface area S of the electrode (middle representation in Scheme S1). This modelling approximation is valid if the constrained diffusion within the pores is assumed to be negligible. The model also assumes a homogeneous distribution of immobile redox active sites O (*i.e.*, $Ti^{IV}O_2$) within the film (with a maximal volumetric concentration C_O^0). Furthermore, due to the excess of inert salt (KCl) systematically added to the electrolyte to maintain a high and near constant ionic strength, it was assumed that the contribution of migration to the charge carrier mass transfer could be neglected. For all species, activities were assimilated to concentrations.

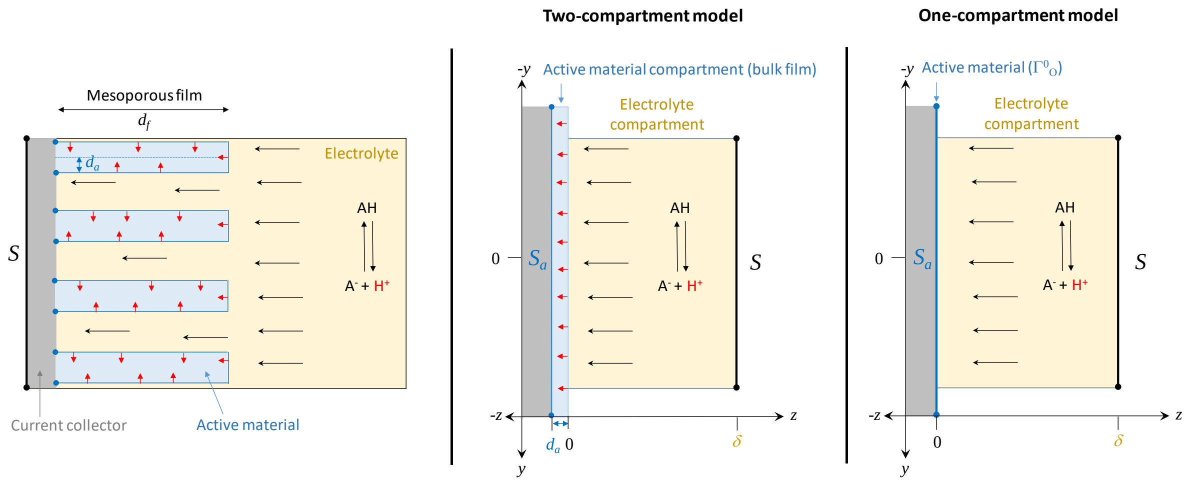

Scheme S1. Schematic representation of (left) the mesoporous GLAD TiO_2 electrode, and its simplified equivalent (middle) two- and (right) one-compartment models. The black arrows symbolize the direction of mass transport of proton donor species present in the electrolyte during electrode reduction, while the red arrows symbolize the directional solid-state mass transport of inserted protons.

On the basis of the two-compartment model (middle representation in Scheme S1), the accessible film thickness for proton diffusion (*i.e.*, along the z-axis $0 > z > d_a$) can be estimated with the following mole conservation law:

$$C_{\mathrm{O}}^{0} S_a d_a = (1-\varepsilon) x C_{\mathrm{O},tot}^{0} S d_f = \Gamma_{\mathrm{O}}^{0} S_a \tag{S1}$$

where ε is the porosity of the film, x a stoichiometric factor indicating the maximal fraction of immobile redox-active sites that can be reduced into RH sites (*i.e.*, $x = C_{\mathrm{O}}^{0} / C_{\mathrm{O},tot}^{0}$), and Γ_{O}^{0} the maximal surface concentration of redox-active sites.

In the case where the mass transport rates for protons and electrons within the TiO_2 film compartment is fast enough to be not rate-limiting, the thin-film compartment (of geometric surface S_a, thickness d_a, and maximal volumetric concentration C_{O}^{0}) can be reduced to a zero-dimensional film of area S_a (localized at $z = 0$) and maximal surface concentration Γ_{O}^{0} (right representation in Scheme S1). As a result, proton migration/diffusion within the solid phase of TiO_2 no longer needs to be considered.

2.2. 1D one-compartment model

2.2.1. *Electrolyte compartment* ($z > 0$)

The electrolyte compartment is filled with a buffered or unbuffered aqueous electrolyte, which consists of a mixture of different proton donor/proton acceptor couples at given concentrations. In the absence of buffer in the electrolyte, there are only two proton donor/proton acceptor couples to consider, *i.e.* H_3O^+/H_2O and H_2O/OH^-, while in the presence of buffer, the additional AH/A^- couple has to be included. All of these species diffuse normal to the electrode (1D linear semi-infinite diffusion along the z-coordinate) with diffusion coefficients D_{AH}, $D_{\mathrm{A^-}}$, $D_{\mathrm{H_3O^+}}$, $D_{\mathrm{H_2O}}$, and $D_{\mathrm{OH^-}}$, respectively. The concentrations C_{AH}, $C_{\mathrm{A^-}}$, $C_{\mathrm{H_3O^+}}$, and $C_{\mathrm{OH^-}}$ rapidly equilibrate through the following acid-base equilibria (water being the solvent, its activity or concentration was considered to be equal to 1):

$$\mathrm{AH} + \mathrm{H_2O} \underset{k_-}{\overset{k_+}{\rightleftarrows}} \mathrm{A^-} + \mathrm{H_3O^+} \qquad \text{with } K_a = k_+ / k_-$$

$$2\,\mathrm{H_2O} \underset{k_{w,-}}{\overset{k_{w,+}}{\rightleftarrows}} \mathrm{OH^-} + \mathrm{H_3O^+} \qquad \text{with } K_w = k_{w+} / k_{w-}$$

where k_{index} are the protonation and deprotonation rate constants (the protonation rate constants can be considered close to the diffusion limit, *i.e.* 10^{10} - 10^{11} $M^{-1}\cdot s^{-1}$ but to avoid convergence problems or excessive computation times during numerical simulations, the protonation rate constants have been adjusted to values 1000-100 times lower, without significantly changing the results). These equilibria are governed by the following thermodynamic equilibrium constants:

$$K_a = \frac{k_+}{k_-} = \frac{C_{\mathrm{A^-}} C_{\mathrm{H_3O^+}}}{C_{\mathrm{AH}}} = 10^{-\mathrm{pH}} \frac{C_{\mathrm{A^-}}}{C_{\mathrm{AH}}} = 10^{-\mathrm{p}K_a}$$

$$K_w = \frac{k_{w,+}}{k_{w,-}} = C_{\mathrm{OH^-}} C_{\mathrm{H_3O^+}} = 10^{-\mathrm{p}K_w}$$

For the electrolyte compartment, we can thus write the following 4 coupled diffusion-convection reaction differential equations:

$$\frac{\partial C_{\mathrm{AH}}}{\partial t} = D_{\mathrm{AH}} \frac{\partial^2 C_{\mathrm{AH}}}{\partial z^2} - k_+ C_{\mathrm{A^-}} C_{\mathrm{H^+}} + k_- C_{\mathrm{AH}} - u \frac{\partial C_{\mathrm{AH}}}{\partial z} \tag{S2}$$

$$\frac{\partial C_{\mathrm{A^-}}}{\partial t} = D_{\mathrm{A^-}} \frac{\partial^2 C_{\mathrm{A^-}}}{\partial z^2} - k_+ C_{\mathrm{A^-}} C_{\mathrm{H^+}} + k_- C_{\mathrm{AH}} - u \frac{\partial C_{\mathrm{A^-}}}{\partial z} \tag{S3}$$

$$\frac{\partial C_{\mathrm{H_3O^+}}}{\partial t} = D_{\mathrm{H_3O^+}} \frac{\partial^2 C_{\mathrm{H_3O^+}}}{\partial z^2} - k_+ C_{\mathrm{A^-}} C_{\mathrm{H_3O^+}} + k_- C_{\mathrm{AH}} - k_{w,+} C_{\mathrm{OH^-}} C_{\mathrm{H_3O^+}} + k_{w,-} - u \frac{\partial C_{\mathrm{H_3O^+}}}{\partial z} \tag{S4}$$

$$\frac{\partial C_{\mathrm{OH^-}}}{\partial t} = D_{\mathrm{OH^-}} \frac{\partial^2 C_{\mathrm{OH^-}}}{\partial z^2} - k_{w,+} C_{\mathrm{OH^-}} C_{\mathrm{H_3O^+}} + k_{w,-} - u \frac{\partial C_{\mathrm{OH^-}}}{\partial z} \tag{S5}$$

where *u* is the convection (or advection) velocity normal to the electrode. (As we will see, this 1D modelling of natural convection is a rough approximation. For a more rigorous consideration, it is necessary to move to a 2D model involving buoyancy effects).

2.2.2. Boundary conditions at the solution-film interface (source terms at z = 0)

2.2.2.1. Faradaic charge storage reaction

At the solution-film interface, proton insertion/disinsertion can only occur *via* one of the following three reversible proton insertion-coupled electron transfer (PICET) reactions or a combination thereof:

$$\mathrm{O + AH + e^-} \underset{}{\overset{E_1^0}{\rightleftarrows}} \mathrm{RH + A^-}$$

$$\mathrm{O + H_3O^+ + e^-} \underset{}{\overset{E_2^0}{\rightleftarrows}} \mathrm{RH + H_2O}$$

$$\mathrm{O + H_2O + e^-} \underset{}{\overset{E_3^0}{\rightleftarrows}} \mathrm{RH + OH^-}$$

Each of these reactions is characterized by its own standard potential, *i.e.* $E_1^0 = E^0_{(\mathrm{O+AH})/\left(\mathrm{RH+A^-}\right)}$, $E_2^0 = E^0_{\left(\mathrm{O+H_3O^+}\right)/(\mathrm{RH+H_2O})}$, $E_3^0 = E^0_{(\mathrm{O+H_2O})/\left(\mathrm{RH+OH^-}\right)}$, as well as by the following standard heterogeneous PICET rate constants, *i.e.* k_1^0, k_2^0, k_3^0, and transfer coefficients, *i.e.* α_1, α_2, α_3, respectively. Phenomenologically, the kinetics of these three interfacial electrochemical insertion reactions can be described by Butler-Volmer expressions for concerted processes, modified here by a Frumkin energetic term in order to take into account the non-ideality resulting from interactions between the intercalation sites in the host lattice:

$$i_{f,1} = -k_1^0 F S_a \exp\left[\alpha_1 g \frac{(C_\mathrm{O})_{z=0}}{C_\mathrm{O}^0}\right] \exp\left[-\frac{\alpha_1 F\left(E - E_1^0\right)}{RT}\right] \left\{ \begin{array}{l} (C_\mathrm{O})_{z=0} (C_\mathrm{AH})_{z=0} \\ -(C_\mathrm{RH})_{z=0} \left(C_{\mathrm{A}^-}\right)_{z=0} \exp\left[-g \dfrac{(C_\mathrm{O})_{z=0}}{C_\mathrm{O}^0}\right] \exp\left[\dfrac{F\left(E - E_1^0\right)}{RT}\right] \end{array} \right\} \quad \text{(S6)}$$

$$i_{f,2} = -k_2^0 F S_a \exp\left[\alpha_2 g \frac{(C_\mathrm{O})_{z=0}}{C_\mathrm{O}^0}\right] \exp\left[-\frac{\alpha_2 F\left(E - E_2^0\right)}{RT}\right] \left\{ \begin{array}{l} (C_\mathrm{O})_{z=0} \left(C_{\mathrm{H_3O^+}}\right)_{z=0} \\ -(C_\mathrm{RH})_{z=0} C^0 \exp\left[-g \dfrac{(C_\mathrm{O})_{z=0}}{C_\mathrm{O}^0}\right] \exp\left[\dfrac{F\left(E - E_2^0\right)}{RT}\right] \end{array} \right\} \quad \text{(S7)}$$

$$i_{f,3} = -k_3^0 F S_a \exp\left[\alpha_3 g \frac{(C_\mathrm{O})_{z=0}}{C_\mathrm{O}^0}\right] \exp\left[-\frac{\alpha_3 F\left(E - E_3^0\right)}{RT}\right] \left\{ \begin{array}{l} (C_\mathrm{O})_{z=0} C^0 \\ -(C_\mathrm{RH})_{z=0} \left(C_{\mathrm{OH}^-}\right)_{z=0} \exp\left[-g \dfrac{(C_\mathrm{O})_{z=0}}{C_\mathrm{O}^0}\right] \exp\left[\dfrac{F\left(E - E_3^0\right)}{RT}\right] \end{array} \right\} \quad \text{(S8)}$$

where $i_{f,1}$, $i_{f,2}$ and $i_{f,3}$ are the faradaic currents generated by each of the three electrochemical PICET reactions, g is a dimensionless constant (Frumkin parameter) characterizing the mean interaction energy between the intercalation sites (positive for repulsion and negative for attraction), and C^0 = 1 M.

The state-of-protonation of the film being given by $\theta = C_\mathrm{RH} / C_\mathrm{O}^0 = \left(C_\mathrm{O}^0 - C_\mathrm{O}\right) / C_\mathrm{O}^0$, equations S6 to S8 can thus be rewritten as follows:

$$i_{f,1} = -k_1^0 F S_a C_\mathrm{O}^0 \exp\left[\alpha_1 g (1-\theta)_{z=0}\right] \exp\left[-\frac{\alpha_1 F\left(E - E_1^0\right)}{RT}\right] \left\{ \begin{array}{l} (1-\theta)_{z=0} (C_\mathrm{AH})_{z=0} \\ -(\theta)_{z=0} \left(C_{\mathrm{A}^-}\right)_{z=0} \exp\left[-g (1-\theta)_{z=0}\right] \exp\left[\dfrac{F\left(E - E_1^0\right)}{RT}\right] \end{array} \right\} \quad \text{(S9)}$$

$$i_{f,2} = -k_2^0 F S_a C_{\mathrm{O}}^0 \exp\left[\alpha_2 g\left(1-\theta\right)_{z=0}\right]\exp\left[-\frac{\alpha_2 F\left(E-E_2^0\right)}{RT}\right]\left\{\begin{array}{l}\left(1-\theta\right)_{z=0}\left(C_{\mathrm{H_30^+}}\right)_{z=0} \\ -\left(\theta\right)_{z=0} C^0 \exp\left[-g\left(1-\theta\right)_{z=0}\right]\exp\left[\frac{F\left(E-E_2^0\right)}{RT}\right]\end{array}\right\} \quad \text{(S10)}$$

$$i_{f,3} = -k_3^0 F S_a C_{\mathrm{O}}^0 \exp\left[\alpha_3 g\left(1-\theta\right)_{z=0}\right]\exp\left[-\frac{\alpha_3 F\left(E-E_3^0\right)}{RT}\right]\left\{\begin{array}{l}\left(1-\theta\right)_{z=0} C^0 \\ -\left(\theta\right)_{z=0}\left(C_{\mathrm{0H^-}}\right)_{z=0} \exp\left[-g\left(1-\theta\right)_{z=0}\right]\exp\left[\frac{F\left(E-E_3^0\right)}{RT}\right]\end{array}\right\} \quad \text{(S11)}$$

It is worth noting that each standard potential is linked to the standard potential of O/RH (*i.e.*, TiO_2/TiOOH) through the pK_a of each proton donor/proton acceptor couple according to:

$$E_1^0 = E^0{}_{\mathrm{O/RH}} - 2.302\frac{RT}{F}\mathrm{p}K_a$$

$$E_2^0 = E^0{}_{\mathrm{O/RH}}$$

$$E_3^0 = E^0{}_{\mathrm{O/RH}} - 2.302\frac{RT}{F}\mathrm{p}K_w$$

From eq. S1, the above equations (S9-S11) can also be rewritten to introduce Γ_{O}^0 and thus better express the relationship with a surface process, appropriate to the 1D one-compartment model:

$$i_{f,1} = -k_1^{0'} F S_a \Gamma_{\mathrm{O}}^0 \exp\left[\alpha_1 g\left(1-\theta\right)_{z=0}\right]\exp\left[-\frac{\alpha_1 F\left(E-E_1^0\right)}{RT}\right]\left\{\begin{array}{l}\left(1-\theta\right)_{z=0}\left(C_{\mathrm{AH}}\right)_{z=0} \\ -\left(\theta\right)_{z=0}\left(C_{\mathrm{A^-}}\right)_{z=0} \exp\left[-g\left(1-\theta\right)_{z=0}\right]\exp\left[\frac{F\left(E-E_1^0\right)}{RT}\right]\end{array}\right\} \quad \text{(S12)}$$

$$i_{f,2} = -k_2^{0'} F S_a \Gamma_{\mathrm{O}}^0 \exp\left[\alpha_2 g\left(1-\theta\right)_{z=0}\right]\exp\left[-\frac{\alpha_2 F\left(E-E_2^0\right)}{RT}\right]\left\{\begin{array}{l}\left(1-\theta\right)_{z=0}\left(C_{\mathrm{H_30^+}}\right)_{z=0} \\ -\left(\theta\right)_{z=0} C^0 \exp\left[-g\left(1-\theta\right)_{z=0}\right]\exp\left[\frac{F\left(E-E_2^0\right)}{RT}\right]\end{array}\right\} \quad \text{(S13)}$$

$$i_{f,3} = -k_3^{0'} F S_a \Gamma_{\mathrm{O}}^0 \exp\left[\alpha_3 g\left(1-\theta\right)_{z=0}\right]\exp\left[-\frac{\alpha_3 F\left(E-E_3^0\right)}{RT}\right]\left\{\begin{array}{l}\left(1-\theta\right)_{z=0} C^0 \\ -\left(\theta\right)_{z=0}\left(C_{\mathrm{0H^-}}\right)_{z=0} \exp\left[-g\left(1-\theta\right)_{z=0}\right]\exp\left[\frac{F\left(E-E_3^0\right)}{RT}\right]\end{array}\right\} \quad \text{(S14)}$$

where $k_1^{0'} = k_1^0 / d_a$, $k_2^{0'} = k_2^0 / d_a$, and $k_3^{0'} = k_3^0 / d_a$.

2.2.2.2. Double-layer electrical capacitance

An additional source term that needs to be included at z = 0 is the capacitive current (i_c) arising from the charging/discharging processes of the two capacitances in series that characterize the TiO_2 film, *i.e.* (1) the charging/discharging of the double-layer capacitance of the conductive TiO_2 film ($C_f = C_{dl} \times S_a$, with C_f the total double-layer capacitance of the film and C_{dl} the differential capacitance), and (2) the exponential filling/emptying of the chemical capacitance (C_{chem}, associated with the injection of electrons in the conduction band and localized states of TiO_2).[S3,S4] C_f is constant, independent of the applied potential, while C_{chem} is function of the applied potential according to the following exponential law:[S3, S5]

$$C_{chem} = \frac{\beta F^2}{RT} d_f C_e^0 \exp\left[-\beta \frac{F}{RT}\left(E - E_{CB}\right)\right] = \frac{\beta F^2}{RT} \Gamma_e^0 \exp\left[-\beta \frac{F}{RT}\left(E - E_{CB}\right)\right] \quad \text{(S15)}$$

where β is a thermodynamic parameter reflecting the energetic distribution of the conduction states of TiO_2, C_e^0 is the maximal volumetric concentration of electrons that can be injected into the semiconductive film (which can also be represented by a surface concentration with $\Gamma_e^0 = d_f C_e^0$), and E_{cb} is the potential of the conduction band of TiO_2 which also depends on the pH as follows: $E_{cb} = E_{cb}^0 - \frac{RT}{F} pH$ (where E_{cb}^0 is the standard conduction band potential, *i.e.* at pH = 0 [S6]).

Assuming that the charge/discharge of double-layer capacitance and chemical capacitance are almost instantaneous, we can therefore apply the following source term for the capacitive current at the solution-film boundary interface (*i.e.*, at z = 0):

$$\frac{i_c}{FS_a} = \frac{1}{\frac{1}{C_{dl}} + \frac{1}{C_{chem}}} \left(\frac{\partial E}{\partial t}\right)_{z=0} \quad \text{(S16)}$$

2.2.2.3. Electrode self-discharge and HER

Although not very significant, the contribution of the self-discharge of the protonated film has been taken into account because it leads to a slight decrease in the Coulombic efficiency, which becomes more pronounced at slower rates.[S2] This self-discharge can be formally described by the spontaneous surface recombination of two inserted protons, leading to the release of H_2:

$$2\,\mathrm{RH} \xrightarrow{k_{self}} 2\,\mathrm{O} + \mathrm{H_2}$$

where k_{self} is the rate constant. The flux of this reaction at $z = 0$ can thus be obtained from:

$$\frac{J_{self}}{S_a} = 2k_{self}\left(\Gamma_{\mathrm{RH}}\right)^2_{z=0}$$

The HER contribution was not considered because it was assumed to be negligible under the experimental conditions we selected for this work, but if required, it can be considered as we have previously done.[S2]

2.2.3. Initial conditions and other boundary conditions

$$t = 0,\ z = 0:\ \Gamma_{\mathrm{O}} = \Gamma^0_{\mathrm{O}} \text{ and } \Gamma_{\mathrm{RH}} = 0 \qquad \text{(S17)}$$

$t = 0,\ z > 0$ and $z = \infty,\ \forall t$:

$$C_{\mathrm{A^-}} = C^0_{\mathrm{A^-}},\ C_{\mathrm{AH}} = C^0_{\mathrm{AH}},\ C_{\mathrm{H_3O^+}} = K_a \frac{C^0_{\mathrm{AH}}}{C^0_{\mathrm{A^-}}} = C^0_{\mathrm{H_3O^+}},\ \text{and}\ C_{\mathrm{OH^-}} = \frac{K_w}{C^0_{\mathrm{H_3O^+}}} = C^0_{\mathrm{OH^-}} \qquad \text{(S18)}$$

(where $C^0_{\mathrm{A^-}}$, C^0_{AH}, $C^0_{\mathrm{H_3O^+}}$ and $C^0_{\mathrm{OH^-}}$ are the initial bulk concentrations in the electrolyte).

$t > 0,\ z = 0$:

The total current is given by the sum of the faradaic and capacitive contributions, *i.e.* $i_t = i_c + i_f$, wherein the faradaic current is given by:

$$\frac{i_f}{FS_a} = \frac{i_{f1} + i_{f2} + i_{f3}}{FS_a} = -\left(\frac{\partial \Gamma_{\mathrm{O}}}{\partial t}\right)_{z=0} = \left(\frac{\partial \Gamma_{\mathrm{RH}}}{\partial t}\right)_{z=0} - \frac{J_{self}}{S_a}$$

and

$$\frac{i_f}{F} = SD_{\mathrm{AH}}\left(\frac{\partial C_{\mathrm{AH}}}{\partial z}\right)_{z=0} + SD_{\mathrm{H_3O^+}}\left(\frac{\partial C_{\mathrm{H_3O^+}}}{\partial z}\right)_{z=0} = -SD_{\mathrm{A^-}}\left(\frac{\partial C_{\mathrm{A^-}}}{\partial z}\right)_{z=0} - SD_{\mathrm{OH^-}}\left(\frac{\partial C_{\mathrm{OH^-}}}{\partial z}\right)_{z=0} \qquad \text{(S19)}$$

2.2.4. Galvanostatic charge/discharge conditions

$0 < t < t_{inv}$: at $z = 0$, $i = -i_g$ (charge)

$t_{inv} < t < t_{max}$: at $z = 0$, $i = i_g$ (discharge)

where i is the total current imposed on the electrode. During a charge/discharge process, this current is split into faradic and capacitive contributions, *i.e.* $i = i_C + i_f$ (where $i_f = i_{f,1} + i_{f,2} + i_{f,3}$).

At $t=0$ and $z=0$, the initial potential (open-circuit potential) of the electrode is given by:

$$E_{eq,i} = E^{0}_{\mathrm{TiO_2/TiOOH}} - 2.302\frac{RT}{F}\mathrm{pH} + \frac{RT}{F}\ln\left(\frac{1-\theta_{eq}}{\theta_{eq}}\right) + \frac{RT}{F}g\left(1-\theta_{eq}\right) \quad \text{(S20)}$$

Because of the slow rates we have used, the effect of the Ohmic drop on the potential was considered to be negligible.

2.3. Multiphysics 2D one-compartment model with buoyancy effects

To more rigorously account for natural convection, and in particular for the buoyancy-driven convection generated by the local change of the electrolyte density at the GLAD TiO_2 electrode, a 2D one-compartment model combining laminar flow fluid dynamics and the aforementioned 1D model (extended to a 2D geometry according to the *y*- and *z*-coordinates) was developed. The 2D geometry was also adjusted to implement the same cell geometry configuration used during the spectroelectrochemical experiments presented in Figures 3 and 4. The layouts of our 2D multiphysics one-compartment model, showing the selected geometry, equations and boundary conditions for mass transport, surface reactions, and laminar flow fluid dynamics are provided in Figure S6 (the nomenclature for parameters and symbols is the same as used in Comsol Multiphysics).

The electrolyte densities reported for diluted solutions of KCl,[S7] KOH and HCl (which for dilute solutions follows a linear relationship with their molar concentration) were used as input parameters (more precisely, the following expression of the electrolyte density at 20°C was used: $\rho = 1.02 + 52\times C_{\mathrm{OH^-}} + 17\times C_{\mathrm{H_3O^+}}$, with ρ in g/cm^3) to calculate the local change of the electrolyte density that triggers buoyancy effects and natural convection through the Navier-Stokes equation for incompressible Newtonian fluids:

$$\rho\frac{\partial u}{\partial t} + \rho\left(u\nabla u\right) = -\nabla p + \mu\nabla^2 u + \rho g \quad \text{(S21)}$$

(where p, μ and g are the pressure, dynamic viscosity, and gravitational force, respectively) and the continuity mass equation:

$$\frac{\partial\rho}{\partial t} + \nabla\left(\rho u\right) = 0 \quad \text{(S22)}$$

Because of the temperature dependence of the electrolyte density, a change of the local density can also be produced by a temperature gradient, however, we considered this effect to be negligible because the cell was thermostatically controlled and low charge/discharge current densities were employed (leading to insignificant energy dissipation at the electrode.

As a result, isothermal conditions were applied to our simulations. On the other hand, since the governing equation S21, only contains information about the pressure gradient, it estimates the pressure field with respect to an unspecified constant. As a result, p was arbitrarily set to zero at a given point in the cell geometry (see Figure S6).

A no-slip boundary condition was assumed to apply to all boundaries, meaning that all velocities are equal to zero at the walls. For the initial conditions, the y- and z-coordinate velocities in the electrolyte domain were also considered to be equal to zero (i.e., no initial convection). The gravity force was set to the y-ordinate. The dynamic viscosity of the 0.5 M KCl electrolyte was obtained from the literature.[S8]

2.4. Procedure for numerical simulations

The above 1D and 2D models were numerically simulated by finite element analysis using COMSOL Multiphysics software (v. 5.5) on a PC computer with Intel Xeon E-2236 CPU, 32 GB RAM and Windows 10 Pro operating system. For the one-compartment 1D model, the “electroanalysis” and “surface reactions” modules were used, while for the one-compartment 2D model involving buoyancy, the “electroanalysis”, “surface reactions”, and “laminar flow” modules were used.

The one-compartment 1D geometry was established as per the schematic in Scheme S1 (right representation), including a one-dimensional electrolyte domain of length δ (chosen as a multiple of the diffusion-convection layer thickness in order to have almost no alteration of the bulk concentrations at this δ boundary). The direct PARDISO solver with a relative tolerance of 10^{-7} was selected. For the mesh element sizes, the maximum and minimum element sizes in the electrolyte domain were 76 µm and 0.877 µm, respectively, with a maximum growth rate of 1.08, while the maximum and minimum element sizes at the level of the boundary electrode were 39.2 µm and 0.117 µm, respectively, with a maximum growth rate of 1.05. A meshing refinement of 3 was also applied to the overall geometry, and the time steps were controlled by the software. In order to include the influence of natural convection that mainly takes place at slow rates, a z-vector velocity field of $u = -5 \times 10^{-3}$ mm/s was set (this value was selected because it limits the growth of the diffusion layer to a maximum thickness of δ_{max} ~250 µm, agreeing with the δ_{max} value reported in ref S9).

As mentioned above, the geometry of the one-compartment 2D model shown in Figure S6 corresponds with the geometric configuration of the spectroelectrochemical cell. The same direct PARDISO solver as for the 1D model was applied with a relative tolerance of 10^{-7}. For the mesh element sizes, the maximum and minimum element sizes in the electrolyte domain and at the level of the boundary electrode were 35.5 µm and 0.1 µm, respectively, with a maximum growth rate of 1.05. A meshing refinement of 5 was also applied to the overall geometry.

3. Estimation of the local pH value at the metal oxide/electrolyte interface on the basis of the simple model of a linear diffusion-convection layer

According to the following proton-coupled charge storage reaction:

$$TiO_2 + x\, e^- + x\, AH \rightleftarrows TiO_2H_x + x\, A^-$$

the insertion/disinsertion of protons during the electrode charge/discharge cycle is associated with the consumption/generation of AH/A^- at the metal oxide/electrolyte interface. Note that because the GLAD-TiO_2 film thickness (1 µm) is small relative to the thickness of the steady-state diffusion-convection layer (δ_{max} is a few hundred µm and it naturally forms over a few tens of seconds in standard electrochemical cells), we can represent the mesoporous electrode as a very thin film located at z = 0, to which the soluble species in the electrolytes diffuse normal to the metal oxide surface (of geometric area S) (Scheme 1). Under the steady-state conditions of natural diffusion-convection, the linear concentration gradients of acid and base that are generated perpendicular to the polarized electrode interface can be described by Fick's first law under the Nernst approximation (*i.e.*, linear gradient):

$$\frac{i_f}{FS} = D_{\mathrm{AH}} \frac{\left(-[\mathrm{AH}]_{z=0} + [\mathrm{AH}]_{\mathrm{bulk}}\right)}{\delta_{\max}} = D_{\mathrm{A^-}} \frac{\left(\left[\mathrm{A^-}\right]_{z=0} - \left[\mathrm{A^-}\right]_{\mathrm{bulk}}\right)}{\delta_{\max}} \tag{S23}$$

where i_f is the faradaic current (in A), F the Faraday constant (96 485 C/mol), $[\mathrm{AH}]_i$ and $[\mathrm{A^-}]_i$ the bulk or local (*i.e.* at z = 0) acid and base concentrations (in mol/cm^3), and D_{AH} and $D_{\mathrm{A^-}}$ are the diffusion coefficients of AH and A^- (in cm^2/s). For the sake of simplicity, the diffusion coefficients of AH and A^- were assumed to be identical and equal to D.

The local pH value at the electrode/electrolyte interface, *i.e.* $\mathrm{pH}_{z=0}$, is thus given by the following expression:

$$\mathrm{pH}_{z=0} = \mathrm{p}K_a + \log\left(\frac{\gamma_{\mathrm{A^-}}}{\gamma_{\mathrm{AH}}}\right)_{z=0} + \log\left(\frac{\left[\mathrm{A^-}\right]_{z=0}}{[\mathrm{AH}]_{z=0}}\right) = \mathrm{p}K_a + \log\left(\frac{\gamma_{\mathrm{A^-}}}{\gamma_{\mathrm{AH}}}\right)_{z=0} + \log\left(\frac{\left[\mathrm{A^-}\right]_{\mathrm{bulk}} + \frac{|i|\delta_{\max}}{FSD}}{[\mathrm{AH}]_{\mathrm{bulk}} - \frac{|i|\delta_{\max}}{FSD}}\right) \tag{S24}$$

Where $\gamma_{\mathrm{A^-}}$ and γ_{AH} are the activity coefficients of the weak base and weak acid, that we can also include into the pK_a constant.

At z = 0, the pH remains equal to the bulk pH as long as both $\left[\mathrm{A}^-\right]_{\mathrm{bulk}}$ and $[\mathrm{AH}]_{\mathrm{bulk}} >> \frac{|i|\delta_{\max}}{FSD}$. According to the model proposed by Amatore and coll.[S9] to account for the role of spontaneous convection in macroscopically immobile solutions (*i.e.*, not subjected to any macroscopic flow or density gradient), a steady-state $\delta_{\max}$ value of ~250 μm was estimated for a redox-active species having a D value of 5.7 × 10^{-6} cm^2/s in an aqueous electrolyte at 25°C. Considering the rate of i/S = -0.36 mA/cm^2 used in the present galvanostatic experiments, this translates into $\frac{|i|\delta_{\max}}{FSD} \approx 2\times10^{-5}$ mol/cm^3. Therefore, no significant pH gradient is expected to develop in the buffered electrolytes used in the present study (prepared with acid and base concentrations >> 0.02 M, thus largely fulfilling the conditions required to avoid the establishment of pH gradients at the electrode/electrolyte interface).

In unbuffered electrolytes containing only a weak Brønsted acid such as the 0.4 M NH_4Cl electrolyte, we have $\left[\mathrm{A}^-\right]_{\mathrm{bulk}} \approx 0$ M and $[\mathrm{AH}]_{\mathrm{bulk}} >> \frac{|i|\delta_{\max}}{FSD}$, which thus enables us to simplify equation S24 into:

$$\mathrm{pH}_{z=0} = \mathrm{p}K_a + \log\left(\frac{\frac{|i|\delta_{\max}}{FSD_{A^-}}}{[\mathrm{AH}]_{\mathrm{bulk}}}\right) \tag{S25}$$

Let us now consider the case of an unbuffered aqueous electrolytes containing a low concentration of a weak Brønsted acid such as, for instance, that used for the experiments in Figure 3 and 4, *i.e.*, aqueous electrolytes containing 0.5 M KCl as inert salt and 0.5 mM phenolphthalein as colorimetric indicator (able to act as a proton donor). Under these conditions, the maximal flux of phenolphthalein (AH) reaching the electrode/electrolyte interface once a steady-state diffusion-convection regime is established can be estimated from the following flux equation:

$$\phi_{AH} = D_{AH}\frac{[\mathrm{AH}]_{\mathrm{bulk}}}{\delta_{\max}^{AH}} \tag{S26}$$

On account of the low concentration of phenolphthalein used, it is reasonable to assume that its concentration at z = 0 remains close to zero. Considering that the diffusion coefficient of phenolphthalein in aqueous solution is ~5 × 10^{-6} cm^2/s and the maximal diffusion-convection layer thickness is ~250 μm, this leads to a calculated flux of $\phi_{AH} \sim 10^{-10}$ $mol/(cm^2 \cdot s)$. To estimate the contribution of phenolphthalein to the proton-coupled charge storage during a glavanostatic cycle, one has to compare this calculated flux to the experimental flux delivered at the electrode interface at a rate of 0.36 mA/cm^2 (equivalent to an electron flux of ~4×10^{-9} $mol \cdot cm^{-2} \cdot s^{-1}$). The 40-fold difference between these two flux values allows us to conclude that the contribution of phenolphthalein as a proton donor in the proton-coupled charge storage is negligible. The same reasoning can also be applied to a 1 mM acetate buffer (which roughly corresponds to a mixture of 0.4 mM acetic acid and 0.6 mM acetate). By this simple calculation, it becomes easy to understand that the proton insertion-coupled charge storage cannot be performed efficiently if the aqueous electrolyte does not contain a sufficient concentration of buffer or proton donor, and that under these conditions, only the aqueous solvent can act as an efficient proton donor.

Table S1. Set of parameters used in the one-compartment 1D model to simulate the galvanostatic curves reported in Figures 2, 5 and 6.

	Parameters	Numerical values
Electrolyte compartment	$D_{AH} = D_{A^-}$ ($cm^2 \cdot s^{-1}$) $D_{H_3O^+}$ ($cm^2 \cdot s^{-1}$) D_{OH^-} ($cm^2 \cdot s^{-1}$) $k_+ = k_{w,+}$ ($M^{-1} \cdot s^{-1}$) u (mm/s) [b]	5×10^{-6} [a] 9.5×10^{-5} [S10,S11] 5.3×10^{-5} [S6,S11,S12] 10^{8} [c] -5×10^{-3}
TiO_2 film	m_{TiO_2} (mg/cm^2) [e] d_a (nm) S_a/S C_O^0 (mol/L) Γ_O^0 (mol/cm^2)	0.25 1.22 540 24 2.93×10^{-9}
Interfacial proton-coupled electron transfer reactions	$k_1^{0'} = k_2^{0'} = k_3^{0'}$ ($cm^3 \cdot mol^{-1} \cdot s^{-1}$) $\alpha_1 = \alpha_2 = \alpha_3$ $E^0_{TiO_2/TiOOH}$ (V) [g] g i_g (mA/cm^2) [e]	82 0.5 -0.7 16 0.36
Capacitance	β E^0_{CB} (V) [g] C_e^0 (mM) C_{dl} ($\mu F \cdot cm^{-2}$) [f]	0.32 0.02 70 55
Self-discharge	k_{self} ($cm^2 \cdot mol^{-1} \cdot s^{-1}$)	13.4×10^{4}

[a] For the NH_4^+/NH_3 couple a slightly faster diffusion coefficient of 2×10^{-5} $cm^2 \cdot s^{-1}$ was used.
[b] Velocity vector used in the 1D model. The value 5×10^{-3} mm/s was selected on the basis that it allows from simulation to produce for a redox species having a diffusion coefficient of 5×10^{-6} cm^2/s a diffusion-convection layer thickness of $\delta_{max} \approx 250$ µm.
[c] To avoid convergence problems or excessive computation times, the protonation rate constants were set to a value 100-fold lower than that reported for a diffusion-controlled reaction (i.e. ~10^{10} $M^{-1} \cdot s^{-1}$).
[e] In per unit of geometric electrode area.
[f] In per unit of accessible electrode area (*i.e.* relative to S_a).
[g] *vs.* NHE.

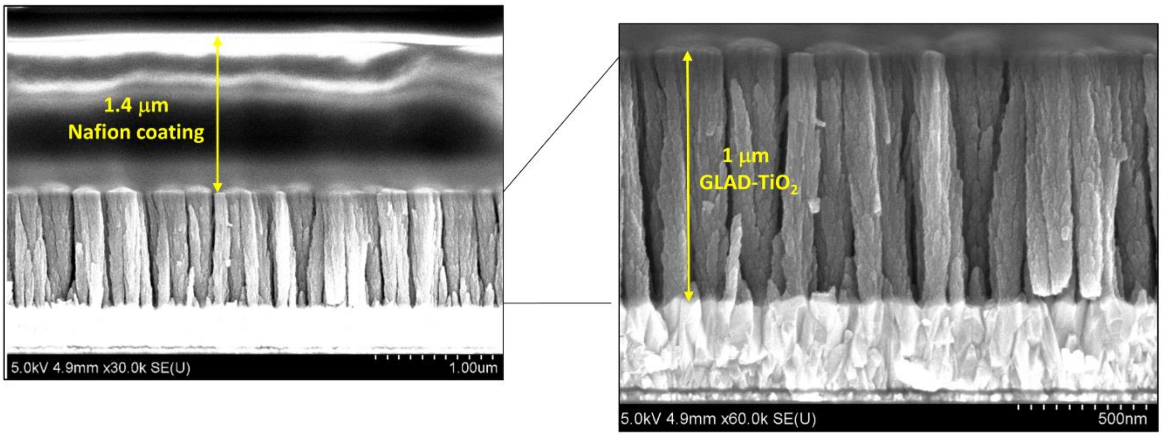

Figure S1. Cross-section SEM images of the Nafion-coated GLAD-TiO_2 electrodes used in the present study. In our previous work, the thickness of the Nafion-coating was estimated to 3 μm. We thus assume some variability in our drop-casting deposition technique.

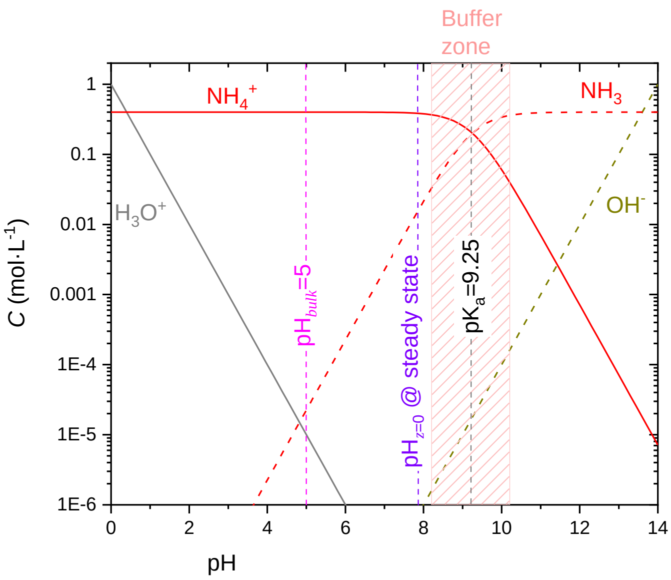

Figure S2. Speciation diagram of the NH_4^+/NH_3 couple (pK_a = 9.25) at a total concentration of 0.4 M in aqueous solution. Calculations were made by equating activities and concentrations.

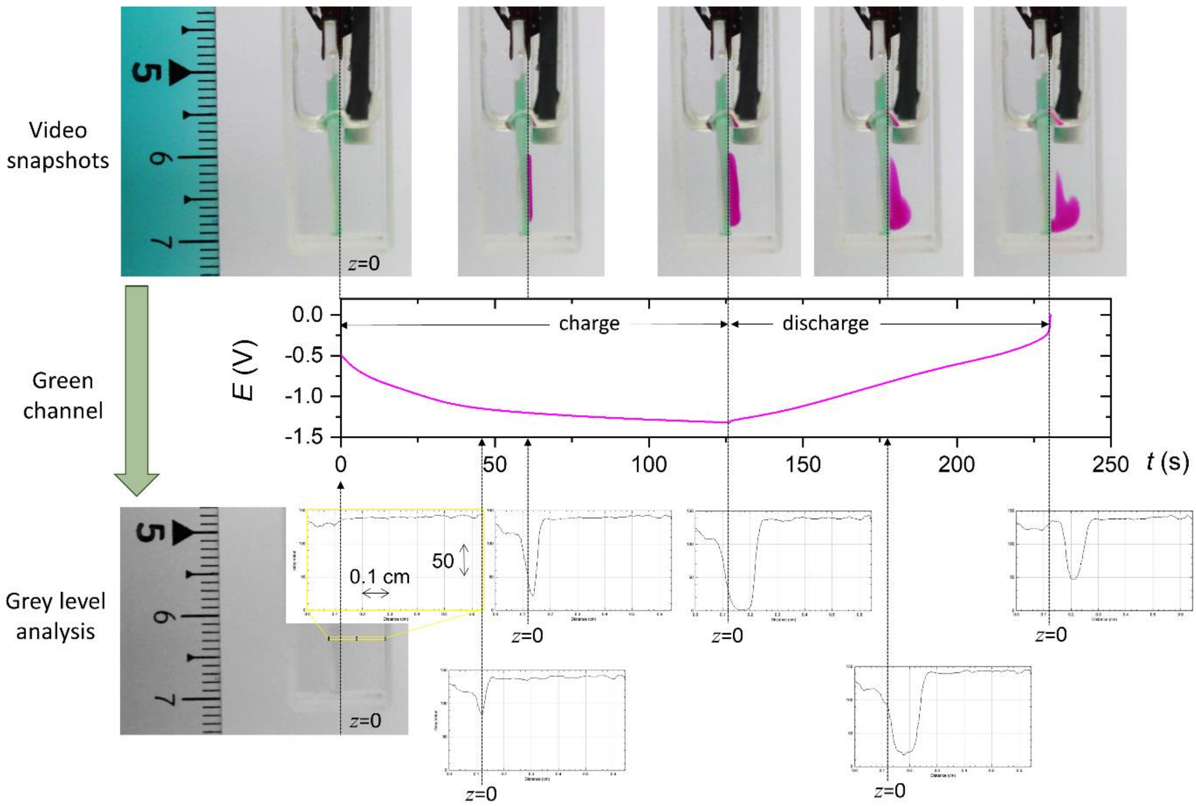

Figure S3. (Top) Video snapshots (extracted from Movie S1) during a galvanostatic cycle carried out at 0.36 mA/cm^2 at a GLAD-TiO_2/FTO electrode in an unbuffered electrolyte containing 0.5 mM phenolphthalein and 0.5 M KCl initially stabilized at pH 5; (bottom) intensity of the green RGB channel over a narrow area delimited by the yellow box extracted from Movie S2 at (from left to right) *t* = 0 s, 46 s, 63 s, 126 s, 178 s, and 228 s. The electrode/electrolyte interface localized at *z*=0 is systematically indicated for proper visualization.

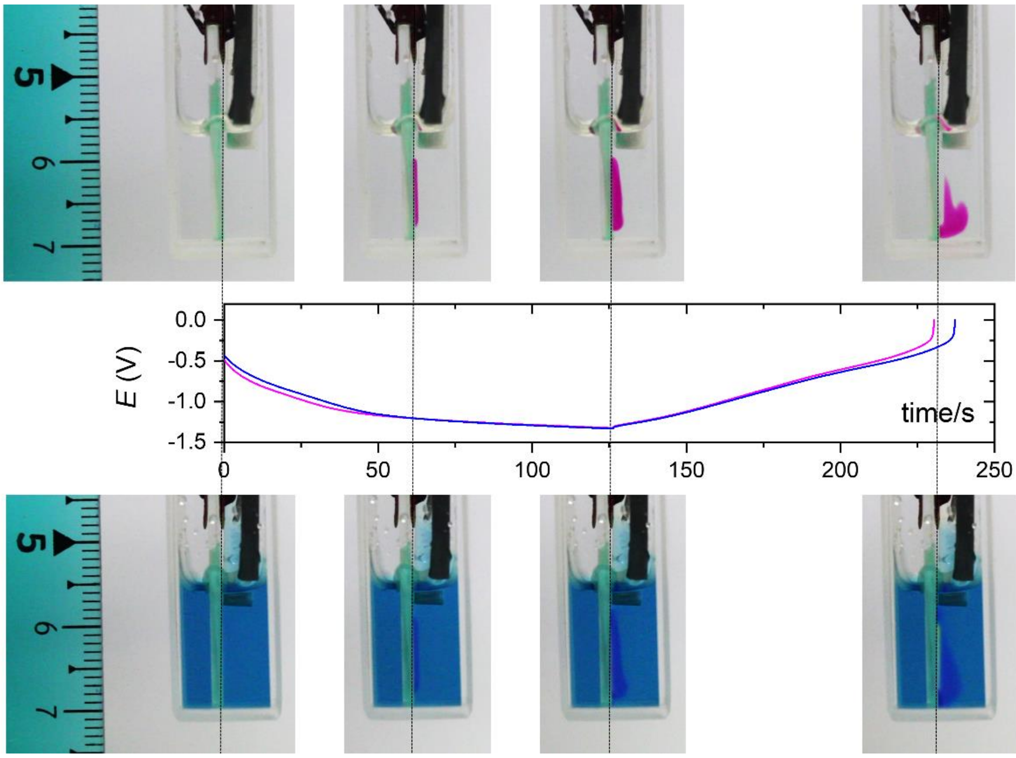

Figure S4. Video snapshots from a galvanostatic cycle carried out at 0.36 mA/cm^2 at a GLAD-TiO_2/FTO electrode in an unbuffered electrolyte containing 0.5 M KCl initially stabilized at pH 5 and (magenta) 0.5 mM phenolphthalein (extracted from Movie S1) or (blue) 0.7 mM bromocresol green (extracted from Movie S3). The electrode/electrolyte interface localized at z=0 is systematically indicated by a dotted line.

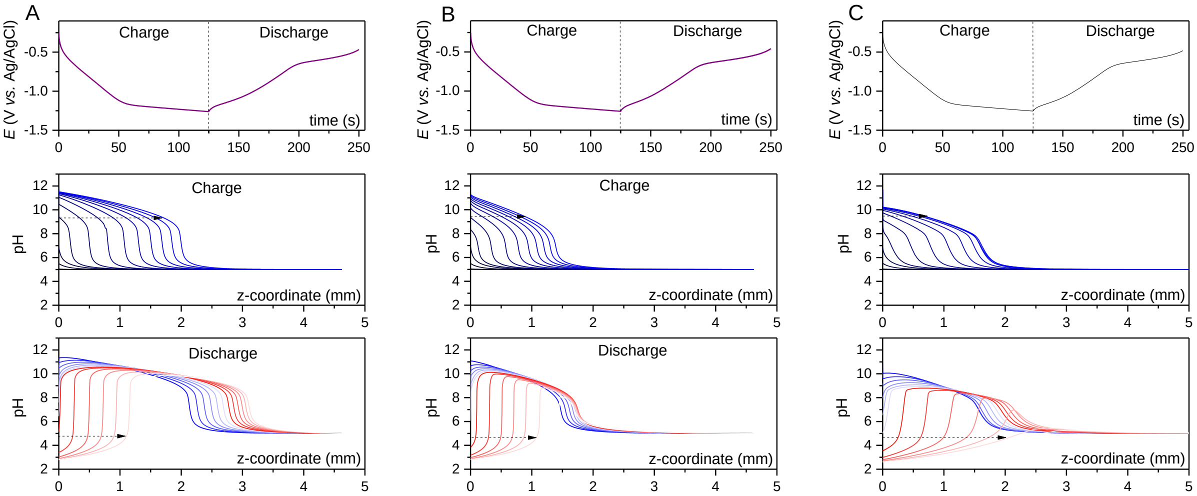

Figure S5. (A) 1D simulations of (top) the galvanostatic charge/discharge cycle in an unbuffered KCl electrolyte (adjusted to pH 5.0), and (middle and bottom) its corresponding pH profiles (here reported every 10 s) along the z-coordinate as a function of time during the (middle) charge and (bottom) discharge processes. The rate (0.36 mA/cm^2) and charge time (126 s) are the same as in the experiment of Figure 4, and the parameters used for simulations are gathered in Table S1. (B) Same as in A but using a 1D simulation model in which the contribution of phenolphthalein (0.5 mM) as a weak acid (pK_a = 9.4) was included. (C) Same as in B but using a 2D simulation model wherein buoyancy effects were incorporated. The dashed horizontal arrows on the middle and bottom graphs are positioned at pH = pK_a of phenolphthalein (9.4) and bromocresol green (4.7), respectively.

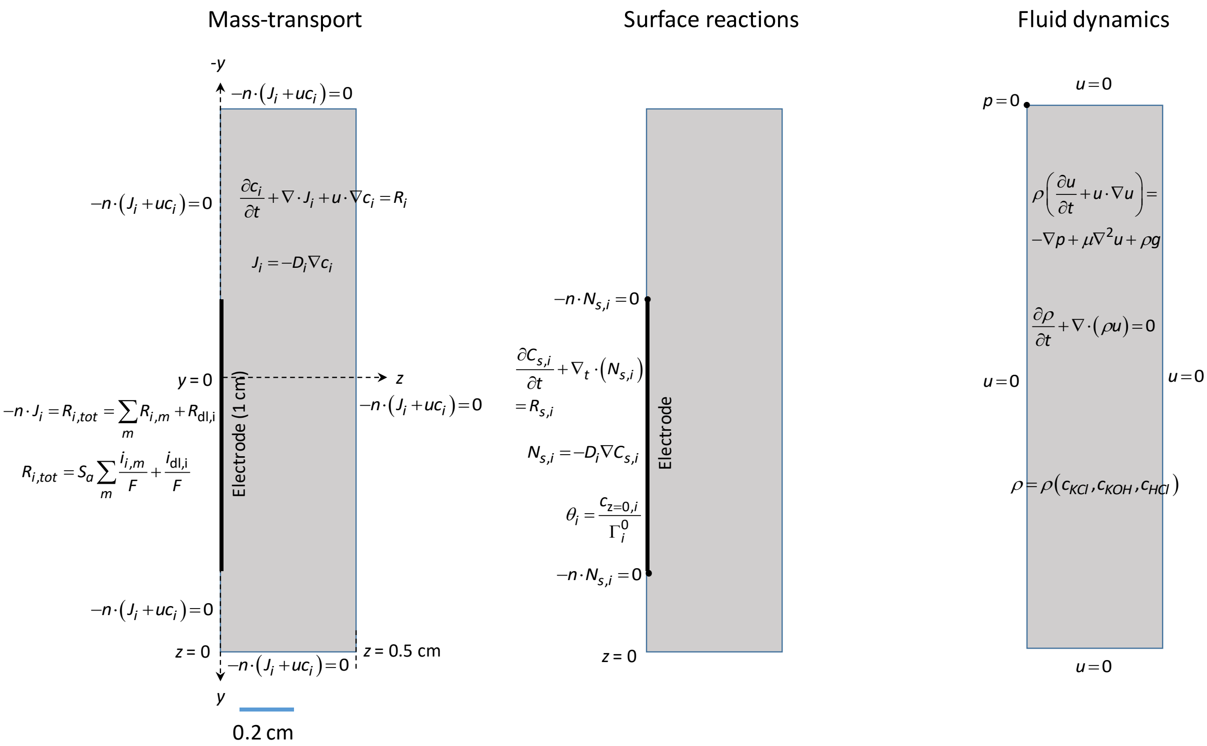

Figure S6. Layouts of the 2D multiphysics one-compartment model, showing the equations and boundary conditions for (left) diffusion-convection mass transport, (middle) surface reactions, and (right) laminar flow fluid dynamics.

References

[S1] Y. S. Kim, V. Balland, B. Limoges, C. Costentin, *Phys. Chem. Chem. Phys.* **2017**, *19*, 17944–17951.

[S2] N. Makivić, J-Y. Cho, K. D. Harris, J-M. Tarascon, B. Limoges, V. Balland, *Chem. Mater.* **2021**, *33*, 3436–3448.

[S3] C. Renault, L. Nicole, C. Sanchez, C. Costentin, V. Balland, B. Limoges *Phys. Chem. Chem. Phys.*, **2015**, *17*, 10592–10607.

[S4] F. Fabregat-Santiago, I. Mora-Seró, G. Garcia-Belmonte, J. Bisquert *J. Phys. Chem. B*, **2003**, *107*, 758–768.

[S5] C. Renault, V. Balland, B. Limoges, C. Costentin, *J. Phys. Chem. C* **2015**, *119*, 14929–14937.

[S6] G. Rothenberger, D. Fitzmaurice, M. Graetzel, *J. Phys. Chem.* **1992**, *96*, 5983–5986.

[S7] J. Kestin, H. E. Khalifa, R. J. Correia, *J. Phys. Chem. Ref. Data* **1981**, *10*, 57–70.

[S8] C. E. Grimes, J. Kestin, H. E. Khalifa, *J. Chem. Eng. Data* **1979**, *24*, 121–126.

[S9] C. Amatore, S. Szunerits, L. Thouin, J. S. Warkocz, *J. Electroanal. Chem.* **2001**, *500*, 62–70.

[S10] V. Grozovski, S. Vesztergom, G. G. Láng, P. Broekmann, *J. Electrochem. Soc.* **2017**, *164*, E3171–E3178.

[S11] H. L. Song, C. R. Jayendran, *J. Chem. Phys.* **2011**, *135*, 124505.

[S12] E. L. Littauer, K. C. Tsai, *Electrochim. Acta* **1979**, *24*, 351–355.